SCIENCE CHINA
Earth Sciences

• RESEARCH PAPER •

January 2014 Vol.57 No.1: 1–15
doi: 10.1007/s11430-014-4928-y

Vegetation physiological parameter setting in the Simple Biosphere model 2 (SiB2) for alpine meadows in the upper reaches of Heihe river

LI Yuan*, SUN Rui† & LIU ShaoMin

[1] *State key laboratory of Remote Sensing Science, co-sponsored by Beijing Normal University and IRSA, Beijing 100875, China;*
[2] *School of Geography, Beijing Normal University, Beijing 100875, China;*
[3] *Beijing Key Laboratory of Environmental Remote Sensing and City Digitalization, Beijing ??, China*

Received January 27, 2014; accepted June 26, 2014

Land surface process modeling of high and cold area with vegetation cover has not yielded satisfactory results in previous applications. In this study, land surface energy budget is simulated using a land surface model for the A'rou meadow in the upper-reach area of the Heihe River Basin in the eastern Tibetan Plateau. The model performance is evaluated using the in-situ observations and remotely sensed data. Sensible and soil heat fluxes are overestimated while latent heat flux is underestimated when the default parameter setting is used. By analyzing physical and physiological processes and the sensitivities of key parameters, the inappropriate default setting of optimum growth and inhibition temperatures is identified as an important reason for the bias. The average daytime temperature during the period of fastest vegetation growth (June and July) is adopted as the optimum growth temperature, and the inhibition temperatures were adjusted using the same increment as the optimum temperature based on the temperature acclimation. These adjustments significantly reduced the biases in sensible, latent, and soil heat fluxes.

SiB2, land surface process, alpine meadow, Heihe River Basin, Tibetan Plateau

Citation: Li Y, Sun R, Liu S M. 2014. Vegetation physiological parameter setting in the Simple Biosphere model 2 (SiB2) for alpine meadows in the upper reaches of Heihe river. Science China: Earth Sciences, 57: 1–6, doi: 10.1007/s11430-014-4928-y

Land surface process is an important part of the mass and energy cycle in the earth system. Dozens of land surface models have been developed in the past 30 years. However, these models do not yield satisfactory results for high-altitude and extremely cold areas, such as the Tibetan Plateau (Yang et al., 2009).

The Tibetan Plateau is a critical region in the land- atmosphere interaction research as it is an important factor in the formation of eastern Asian summer monsoon (Song et al., 2010; Yanai et al., 1992). It is often addressed as the "Third Pole" of the world (Qiu, 2008) because its climatic features and geographical significance are similar to those of the Arctic and Antarctic. The Tibetan Plateau has some unique features as a result of its high altitude, extreme environment, and climate. Yang et al. (2009) summarized three main characteristics of the Tibetan Plateau: i) strong diurnal change in the surface energy budget owing to strong solar heating, ii) contrast between the dry western region and the wet eastern region, and iii) significant seasonal variation in the surface energy budget in the central and eastern regions.

Owing to the spatial disparity of the climate, the western region is characterized by alpine deserts, whereas the eastern region is covered with alpine meadows and grasslands, e.g., the meadows in upper-reach area of the Heihe River

*Corresponding author (email: yuan.li2@monash.edu);
†Corresponding author (email: sunrui@bnu.edu.cn)

Basin. In the western Tibetan Plateau, radiation and energy balances are strongly influenced by snow cover, permafrost, and sporadic precipitation. Conversely, in the eastern and central Tibetan Plateau, the precipitation is relatively plenty in summer due to the monsoon. Therefore, the land surface processes in the warm season are different from those in the cold season. Soil freezing and thawing strongly affects energy exchange in spring and autumn, whereas in summer, vegetation plays an important role in surface water and energy balances.

To better understand land surface processes in extremely high-cold regions, many land-atmospheric field experiments have been conducted, e.g., the Global Energy and Water cycle Experiment-Asian Monsoon Experiment-Tibet (GAME/Tibet) (Koike et al., 1999), the Tibetan Plateau Experiment of Atmospheric Sciences (TIPEX) (Zhang et al., 2000), the CEOP Asia-Australia Monsoon Project in Tibet (CAMP/Tibet) (Koike, 2004), the New Integrated Observational System over the Tibetan Plateau (NIOST) (Xu et al., 2008), the Tibetan Observation and Research Platform (TORP) (Ma et al., 2008), the Watershed Allied Telemetry Experimental Research (WATER) (Li et al., 2009), and the ongoing Heihe Watershed Allied Telemetry Experimental Research (HiWATER) (Li et al., 2013).

These experiments and projects have extended our understanding of the characteristics of the land surface process at high-altitude regions. A number of land surface modeling studies have been conducted in the past 20 years based on the observed data from these experiments. Some studies have focused on the impact of snow cover and soil freezing-thawing process on land surface radiation, energy, and water balance (Hu et al., 2006; Li and Sun, 2008; Li et al., 2010; Takayabu et al., 2001; Yasunari et al., 2011; Zhou and Huang, 2012), and some researchers have emphasized the impact of energy exchange between different soil layers on the entire energy transfer process (Gao et al., 2007; van der Velde et al., 2009; Yang et al., 2005). Based on experimental data, a scheme for parameterizing the thermal roughness length has been developed (Yang et al., 2002) and applied in a land surface model and this scheme significantly reduces biases in simulated surface energy budget and surface temperature of the western Tibetan Plateau (Chen et al., 2010, 2011). Several studies also discussed the role of vegetation in land surface energy partition for alpine meadows (Gao et al., 2002; Gao et al., 2004; Hong and Kim, 2010; Yang et al., 2004). Some of these studies show that the energy balance for the central and eastern Tibetan Plateau during the wet period could not be simulated well by land surface models. For instance, Gao et al. (2002) adopted the Simple Biosphere model 2 (SiB2) to simulate surface energy budget using data from an automatic weather station, field survey, and remote sensors at the Naqu BJ site in the central Tibetan Plateau. By comparing their results with eddy covariance observations during the vegetation growth season, they found that the SiB2 model overestimated the sensible heat. However, explanations of the bias in model simulations for the eastern and central Tibetan Plateau remain lacking.

In this study, a land surface modeling experiment is conducted for A'rou alpine meadow in the upper-reach area of the Heihe River Basin in the eastern Tibetan Plateau using a new version of SiB2 model, to further address the impact of the unique climate and vegetation features of alpine meadows. The land surface energy balance is evaluated and erroneous vegetation parameters are identified through energy exchange process analysis and parameter sensitivity test. A new vegetation parameter setting scheme is implemented subsequently improving the model performance.

1 Data and Methods

1.1 Site and data

This study is conducted at the A'rou observation site (38°02′39.8″N, 100°27′52.9″E), an experimental site in WATER (Li et al., 2009) and HiWATER program (Li et al., 2013), in Qilian County, Qinghai Province. The site is located in a valley with a maximum width of 3 km upstream of the Heihe River Basin to the northeast of the Tibetan Plateau. It is a typical alpine meadow site with relatively homogeneous coverage. The terrain around the observation site is relatively flat, with a gentle slope from the southeast to the northwest, which makes it ideal for land surface modeling and validation. The A'rou meadow is an extremely high-cold region, located at an elevation of 3030 m. The annual precipitation and mean air temperature are 405 mm and 1.0°C, respectively (observation of Qilian station, 1957–2008)[1)]. Figure 1 shows the seasonal variations and the inter-annual changes in precipitation and mean air temperature (K) for the A'rou meadow. The soil is silt loam, and it starts to freeze in October every year and may not completely thaw until May the next year. However, during summer, grass grows quickly to a maximum height of proximately 20–30 cm, which changes the land water and energy partition pattern.

The observation instruments at A'rou site include an automatic weather station (AWS), an eddy covariance (EC) system, and a large aperture scintillometer (LAS). The AWS is installed at the middle of the observation field for recording wind direction, wind velocity, air temperature, air pressure, air humidity, precipitation, radiation, soil heat flux, and soil temperature and moisture. The EC system is installed near the AWS to record high-frequency fluctuation of wind, temperature, and humidity, which are used to calculate sensible and latent heat fluxes. The transmitter and receiver of LAS are installed at the north side and south side

1) Data obtained from China Meteorological Data Sharing Service System (http://cdc.cma.gov.cn/)

of the valley, respectively, to observe the sensible heat flux. Detailed information of these instruments is provided in Table 1. For a more detailed description of the site and the data processing process, refer to Liu et al. (2011) and Li et al. (2009).

All data used in this study are collected from 11 June to 30 September 2008, averaged over hourly intervals. The winter season is not considered to avoid the effect of the freeze-thaw process, which is not well represented in the standard version of SiB2 (Li and Koike, 2003; Yang et al., 2009). Short wave radiation (downwards), long wave radiation (downwards), wind velocity, air temperature, air humidity, and precipitation recorded by the AWS are used as forcing data. Net radiation observed by the AWS, sensible and latent heat fluxes observed by EC system, and soil heat flux are used as validation data. By considering the ordinary linear regression slope of turbulent energy fluxes (H+LE) versus the available energy (R_n-G_0) as the energy balance closure ratio (Wilson et al., 2002), the ratios for both the daytime and the entire day at the A'rou site during June to September 2008 are about 87%, which is close to the value calculated by Liu et al. (Liu et al., 2011). The accuracy of the soil heat flux plate observations is affected by the buried depth and the sensitivity of the plates, and hence, in this study, we calculate the soil heat flux from the soil temperature and moisture observations using the thermal diffusion equation-correction (TDEC) method (Yang and Wang, 2008).

1.2 Model and parameter setting

The SiB2 model was developed by Sellers et al. (1996b) based on the SiB model. It incorporates a canopy photosynthesis conductance sub-model to simulate a more realistic vegetation physiological process.

It simplifies the two-story vegetation used in the first version of SiB to a single layer to fully use the remote sensing data. It also improves the snow cover and hydrological process simulation. As one of the most influential land surface models, the SiB2 model has been widely implemented in regional and global land surface modeling (Gao et al., 2004; Hanan et al., 2005; Prihodko et al., 2008; Sen et al., 2000; Yang et al., 2009).

For this study, we adopted all modules of the SiB2 model except for the calculation of aerodynamic parameters used in the canopy transfer resistances parameterization. In the SiB2 model, these aerodynamic parameters are calculated using a K-theory based model, which is inconsistent with the classic mixing-length theory when aerodynamic roughness length (z_0) approaches the bare-soil value (Yang et al., 2009). In the present study, we incorporate a mixing-length theory based canopy model (Watanabe and Kondo, 1990) to calculate the aerodynamic parameters.

There are three main types of parameters in the SiB2 model, namely, vegetation, soil, and topographical parameters. Topographical and vegetation morphologic parameters

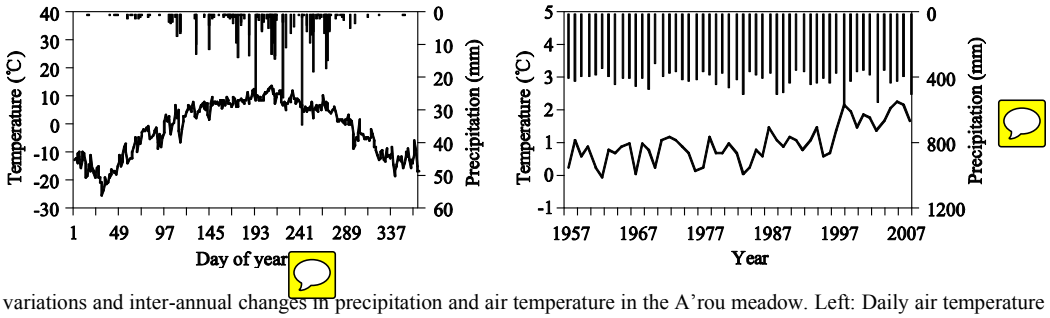

Figure 1 Seasonal variations and inter-annual changes in precipitation and air temperature in the A'rou meadow. Left: Daily air temperature and precipitation in 2008; Right: Annual air temperature and precipitation from 1957 to 2008. The curves represent temperatures and the bars represent precipitation.

Table 1 Description of the instruments incorporated in the AWS, EC system, and LAS at A'rou site

Instruments	Variable	Sensors	Height/Depth(m)
AWS	Air temperature/humidity	HMP45C, Vaisala	2.07, 10.04
	Wind velocity	014A, Met One	2.03, 10.16
	Wind direction	034B, Met One	10.16
	Air pressure	CS105, Vaisala	/
	Precipitation	TE525, Campbell	/
	Radiation	PSP&PIR, Eppley	1.50
	Soil heat flux	HFT3, Campbell	0.05, 0.15
	Soil temperature	107, Campbell	0.1, 0.2, 0.4, 0.8, 1.2, 1.6
	Soil moisture	CS616, Campbell	0.1, 0.2, 0.4, 0.8, 1.2, 1.6
EC	Sensible and latent heat flux	CSAT3, Campbell and Li7500, Li-cor	3.15
LAS	Sensible heat flux	BLS450, Scintec	9.5

along with soil depths and porosities are set based on prior knowledge and field survey data. LAI (leaf area index) and vegetation cover are derived from monthly averaged MODIS (moderate-resolution imaging spectroradiometer) products. Other parameters are set to default values obtained from Sellers et al. (1996a). Table 2 lists the parameter values used in this study. The vegetation height parameters are much smaller than the default values for vegetation type 6 by Sellers et al. (1996a), which indicates the unique characteristics of vegetation in the Tibetan Plateau. The measured soil porosity is relatively high yet close to measurements presented in a recent study by Chen et al. (2012).

The initial values of the state variables are calculated from the observed data, including air (canopy) temperature and humidity, and soil temperature and moisture.

2 Energy balance simulation and uncertainty identification

Based on the parameter setting described above, the energy budget for the A'rou meadow is simulated using the SiB2 model. To avoid the freezing and thawing process, which is not described in the SiB2 model (Sellers et al., 1996b; Yang et al., 2009), the energy balance is only simulated and evaluated from 11 June to 30 September 2008.

Figure 2 shows the monthly averaged daily variation in each surface energy budget component. As expected, the net radiation simulations are quite consistent with the observations. However, the sensible and latent heat fluxes tend to be overestimated and underestimated, respectively, compared with the observations. The biases in the heat flux simulations are observed mainly in the data collected during the daytime. The soil heat flux is slightly overestimated. To further examine the biases in the sensible and latent heat fluxes in the daytime data, the scatter plots and linear regression equations of the surface energy budget simulated using the SiB2 model are shown against the observations during the unstable stratification condition (daytime) in Figure 3. The net radiation simulations and observations approximately follow the 1:1 line, and the determination coefficient R^2 is close to 1. This result indicates that the SiB2 model has a high capability of radiation balance simulation, and the values of surface spectral character parameters are appropriate.

The sensible, latent and soil heat fluxes simulated for an unstable stratification condition have different levels of bias. The sensible and soil heat fluxes are overestimated by 28% and 7.7%, respectively, while the latent heat flux is underestimated by 12% compared with the observations. However, due to the lack of energy balance closure widely existing in EC measurements, the bias of latent heat flux may have been underestimated. As mentioned earlier, the energy balance ratio at the A'rou site during June to September 2008 is about 87%, which indicates that the underestimation

Table 2 Parameter setting for the SiB2 model at A'rou site[a)]

	Parameter	Value		Parameter	Value
z_2*	Canopy-top height (m)	0.2	V_{max0}	Maximum rubisco capacity, top leaf (mol m^{-2} s^{-1})	3×10^{-5}
z_1*	Canopy-base height (m)	0.02	ε	Intrinsic quantum efficiency (mol mol^{-1})	0.05
z_c*	Inflection height for leaf-area density (m)	0.08	G_1	Augmentation factor for momentum transfer coefficient	1.449
z_s*	Ground roughness length (m)	0.005	G_4	Transition height factor for momentum transfer coefficient	11.785
χ_L	Leaf-angle distribution factor	–0.3			
l_w*	Leaf width (m)	0.008	m	Stomatal slope factor	4.0
l_l*	Leaf length (m)	0.08	b	Minimum stomatal conductance (mol m^{-2} s^{-1})	0.04
D_T*	Total soil depth (m)	1.5	β_{ce}	Photosynthesis coupling coefficient	0.8
D_r*	Root depth (m)	0.4	β_{ps}	Photosynthesis coupling coefficient	0.95
D_1*	Depth of surface soil layer (m)	0.05	ψ_c	One-half inhibition water potential (m)	–200
$\alpha_{V,l}$	Leaf reflectance, visible, live	0.105	f_d	Leaf respiration factor	0.025
$\alpha_{V,d}$	Leaf reflectance, visible, dead	0.36	s_1	High temperature stress factor, photosynthesis (K^{-1})	0.3
$\alpha_{N,l}$	Leaf reflectance, near IR, live	0.58	s_2	Half-inhibition high temperature, photosynthesis (K)	313
$\alpha_{N,d}$	Leaf reflectance, near IR, dead	0.58	s_3	Low temperature stress factor, photosynthesis (K^{-1})	0.2
$\delta_{V,l}$	Leaf transmittance, visible, live	0.07	s_4	Half-inhibition low temperature, photosynthesis (K)	288
$\delta_{V,d}$	Leaf transmittance, visible, dead	0.22	s_5	High temperature stress factor, respiration (K^{-1})	1.3
$\delta_{N,l}$	Leaf transmittance, near IR, live	0.25	s_6	Half-inhibition high temperature, respiration (K)	328
$\delta_{N,d}$	Leaf transmittance, near IR, dead	0.38	T_{opt}	Optimum temperature for vegetation growth (K)	298
$\alpha_{s,V}$	Soil reflectance, visible	0.1	B	Soil wetness exponent	5.39
$\alpha_{s,N}$	Soil reflectance, near IR	0.2	ψ_s	Soil tension at saturation (m)	–0.15
z_{win}*	Wind observation height (m)	2.03	K_s	Hydraulic conductivity at saturation (m s^{-1})	7.0×10^{-6}
z_{win}*	Air temperature and humidity observation height (m)	2.07	θ_s*	Soil porosity (volume fraction)	0.60
L_T**	Leaf area index	1.9, 3.3, 3.3, 1.3	V**	Vegetation cover (%)	67, 95, 94, 78

a) Items with marked by * are set based on prior knowledge and field survey. Items marked by ** are monthly mean data from June to September, 2008. Others are obtained from Sellers et al. (1996a).

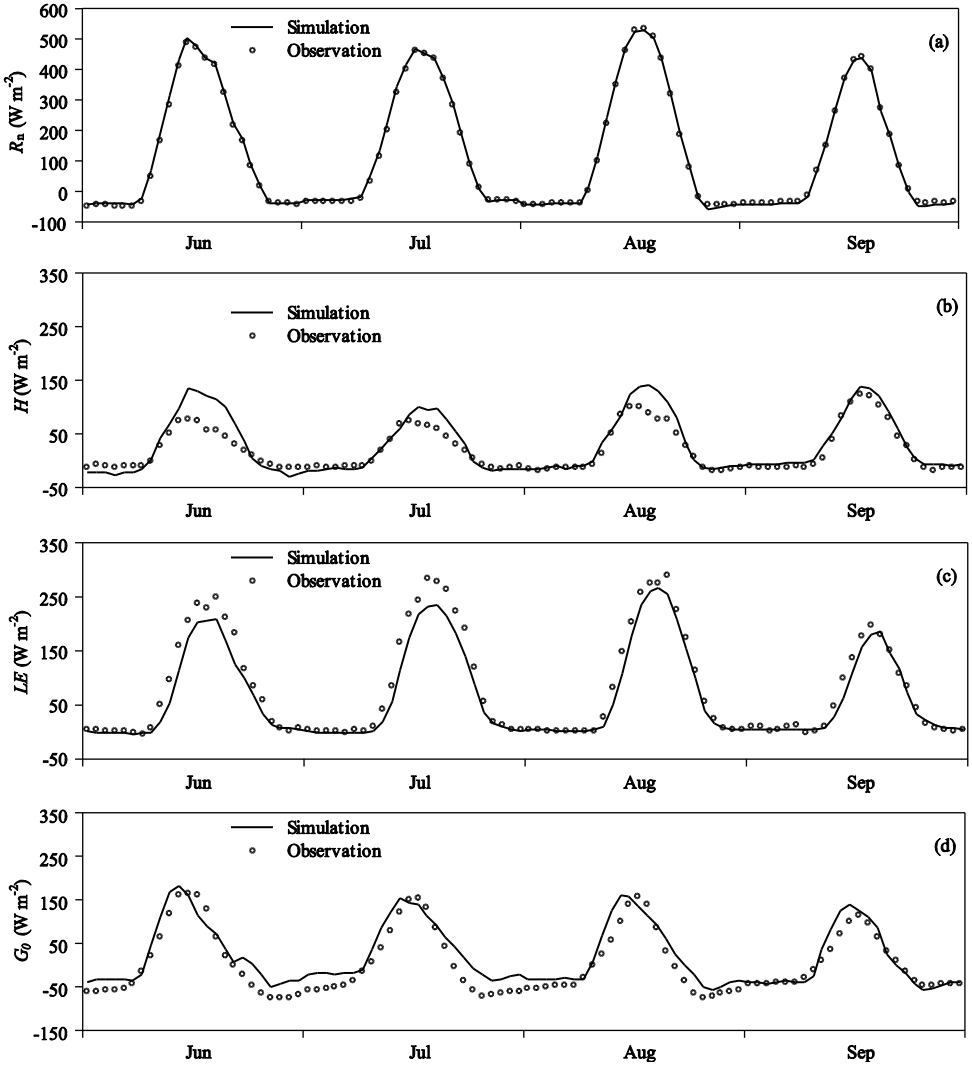

Figure 2 Comparison of simulated monthly-mean diurnal variations of surface energy budget against observations

of latent heat flux may be greater than 12% and the overestimation of sensible heat flux may be less than 28%. The bias in surface energy fluxes in the Tibetan Plateau was also identified in some past studies. For example, Gao et al. (2002) found that the SiB2 overestimates the sensible heat flux at Naqu.

On all accounts, after using in-situ observed data, remotely sensed data, and default values from Sellers et al. (1996a) for model parameter setting and states initialization, the modeled sensible heat flux shows a positive bias and latent heat flux shows a negative bias to some extent. As the parameterization scheme of heat flux in the SiB2 model is based on the energy balance equation shown in eqs. (1a) and (1b), the calculation error of either the sensible heat flux or the latent heat flux will affect the other. Therefore, we analyzed the simulated sensible and latent heat fluxes sequentially to identify the source of the bias.

$$C_c \frac{\partial T_c}{\partial t} = R_{nc} - H_c - LE_c - \xi_{cs}, \quad (1a)$$

$$C_g \frac{\partial T_g}{\partial t} = R_{ng} - H_g - LE_g - \frac{2\pi C_d}{\tau_d}(T_g - T_d) - \xi_{gs}, \quad (1b)$$

where T_c, T_g and T_d are temperatures (K); R_{nc} and R_{ng} are net radiations (W m^{-2}); H_c and H_g are sensible heat fluxes (W m^{-2}); LE_c and LE_g are latent heat fluxes (W m^{-2}); C_c, C_g and C_d are effective heat capacities (J m^{-2} K^{-1}); τ_d is the daylength (s); ξ_{cs} and ξ_{gs} are energy transfers due to phase changes (W m^{-2}). The subscript "*c*" refers to the canopy, "*g*" to the soil surface, "*d*" to deep soil.

2.1 Process analysis on sensible heat flux overestimation

The uncertainty of the sensible heat flux estimation in the SiB2 model may arise from two components: the aerodynamic resistances (r_a, r_b, and r_d) and the potential difference between the surface and air temperatures.

$$H_c = (T_c - T_a)\rho c_p / r_b, \quad (2a)$$

$$H_g = (T_g - T_a)\rho c_p / r_d , \quad (2b)$$

$$H_c + H_g = (T_a - T_m)\rho c_p / r_a . \quad (2c)$$

where T_a is the canopy air temperature (K); T_m is the air temperature at an observing height (K); ρ is the density of air (kg m^{-3}); c_p is the specific heat of air (J kg^{-1} K^{-1}); r_b is the bulk canopy boundary layer resistance (s m^{-1}); r_d is the aerodynamic resistance between ground and canopy air space (s m^{-1}); r_a is the aerodynamic resistance between canopy air space and reference height (s m^{-1}).

In the SiB2 model, the calculation of aerodynamic resistances are affected by atmospheric boundary-layer wind speed (u_m), canopy top wind speed (u_2), aerodynamic roughness length (z_0), bulk boundary-layer resistance coefficient (C_1) and ground to canopy air-space resistance coefficient (C_2). u_m is measured and u_2 is calculated from u_m. z_0, C_1, and C_2 are calculated through a canopy model based on the mixing-length theory (Watanabe and Kondo, 1990) using observed vegetation structure parameters. These calculations are relatively rigorous in theory.

$$r_b = C_1 / (u_2)^{1/2} , \quad (3a)$$

$$r_d = C_2 / u_2 , \quad (3b)$$

$$r_a = \frac{C_3}{u_m} \approx \left[\frac{1}{k} \log\left(\frac{z_m - d}{z_0} \right) \right]^2 / u_m . \quad (3c)$$

where C_3 is the aerodynamic (canopy air-space to reference height) resistance coefficient; k is the von Karman constant; d is the zero plane displacement height (m); z_m is the atmospheric boundary-layer reference height (m).

Table 3 presents the values of z_0, C_1, and C_2 for the A'rou meadow from June to September 2008 calculated from the mixing-length theory. The value of z_0 is reasonable according to its order of magnitude. The values of C_1 and C_2 are also within the normal range for alpine meadows according to a sensitivity analysis of Tibetan short grass prairie in the GAME/Tibet experiment conducted by Gao et al. (2002). Nevertheless, we tested the sensitivities of sensible heat flux to z_0, C_1, and C_2, by artificially decreasing z_0 and increasing C_1 and C_2. As shown in eq. (3), decreasing z_0 and increasing C_1 and C_2 can increase the aerodynamic resistances. Table 4 gives the linear regression slope of the modeled sensible heat flux against EC measurements (for unstable stratification). It shows that the sensible heat flux simulations do not benefit much from the adjustment of z_0 and C_1. The linear regression slope of sensible heat flux decreased from 1.23 to 1.15, which indicates that the overestimation of sensible heat flux decreases from 27.7% to 15.4% by the positive adjustment of C_2. However, a comparison of the linear regression slopes of latent and soil heat fluxes with observations (Table 5) shows that the latent heat flux is not sensitive to positive adjustment of C_2, while the soil heat flux has a comparatively obvious increase. The linear regression slope of soil heat flux increases from 1.08 to 1.16, which implies that the positive adjustment of C_2 will indeed decrease the sensible heat flux. However, the reduced portion of energy has not been added to the latent heat flux but to the soil heat flux. Thus, C_2 mainly affected the energy allocation between the sensible and soil heat fluxes, which is not a problem encountered in this research. In conclusion, the main uncertainty in SiB2 is not introduced because of aerodynamic parameters.

Another factor affecting the sensible heat flux is the difference between surface and air temperatures. Since the AWS records air temperature at a reference height, and this

Table 3 z_0, C_1, and C_2 calculated from the mixing-length theory

	June	July	August	September
z_0 (mm)	24.2	25.4	25.4	22.6
C_1	19.8	17.6	17.6	22.8
C_2	84.8	87.5	87.5	82.2

Table 4 The sensitivities of sensible heat flux against z_0, C_1, and C_2 (for unstable stratification)[a)]

	Original value	50% negative bias added to z_0	100% positive bias added to C_1	100% positive bias added to C_2
Regression slope	1.28	1.28	1.25	1.15

a) The regression slope is the linear regression slope between simulations and observations, which is equivalent to the coefficient of x in Figure. 3. Ideally it should be 1.

Table 5 The sensitivity of latent and soil heat flux against C_2 (for unstable stratification)

	Original value	100% positive bias added to C_2
Regression slope of LE	0.88	0.87
Regression slope of G_0	1.08	1.16

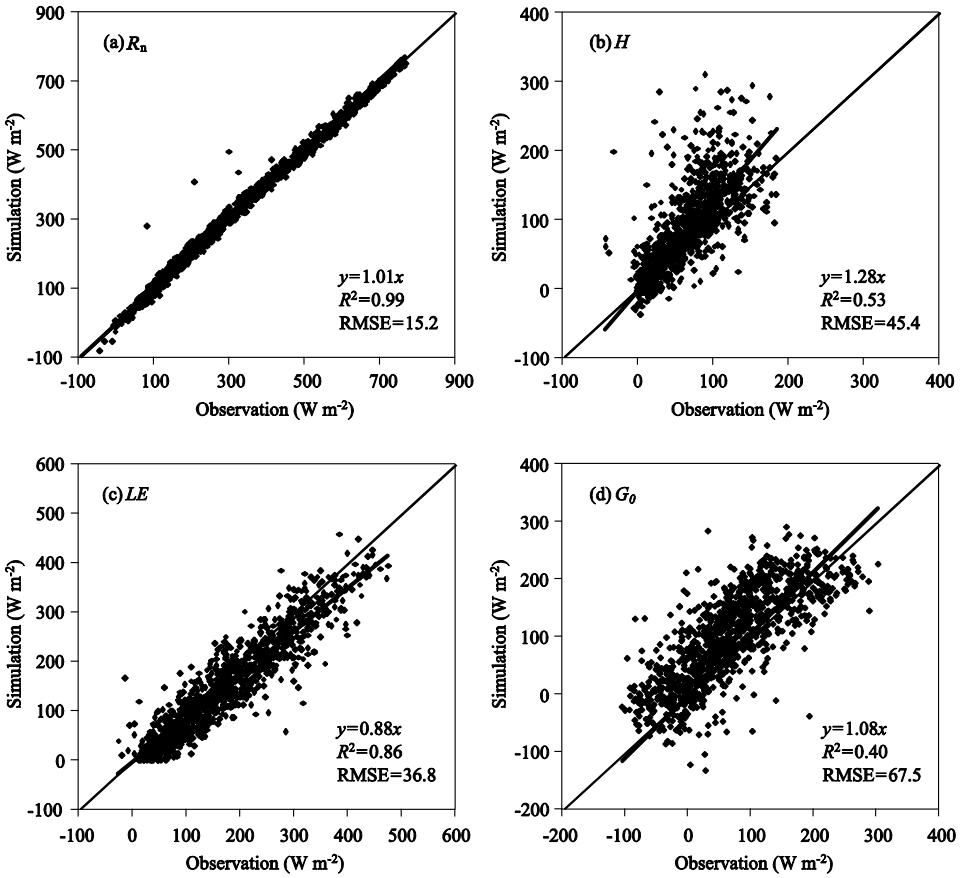

Figure 3 Scatter plots of surface energy budget modeled by the SiB2 model against observations in unstable stratification condition (daytime)

measurement is assumed to be unbiased. Thus, the key factor is the simulation of land surface temperature. Surface temperature in the SiB2 model is estimated as two independent state variables, namely, vegetation canopy temperature and surface soil temperature, which are difficult to evaluate separately. Here, we derived the surface temperatures from long-wave radiations based on the Stefan-Boltzmann law considering environmental radiation contribution. To ensure that the results are comparable and to avoid the impact of the uncertainty in the emissivity, the observed surface temperature is calculated from observed long wave radiations and simulated surface temperature is calculated from the simulated long wave radiations.

$$R_{lu} = \varepsilon\sigma \cdot T^4 + (1-\varepsilon)R_{ld}\,. \tag{4}$$

where R_{lu} and R_{ld} are the upward and downward long wave radiations, respectively. The land surface emissivity ε is set to 0.985 based on the underlying surface condition and the Stefan-Boltzmann constant σ is 5.67×10^{-8} W m^{-2} K^{-4}.

Figure 4 compares the simulated and observed monthly mean diurnal variations in the potential difference between surface and air temperatures. There is no obvious overestimation of this difference. According to eqs. (1a) and (1b), the canopy and soil temperatures are two state variables, and they are restricted by the energy balance. Any uncertainty in the sensible or latent heat fluxes can cause uncertainty in the surface temperature. Therefore, it is difficult to conclude whether the sensible heat flux estimation module or the latent heat flux estimation module is the dominant factor causing the bias based solely on the temperature

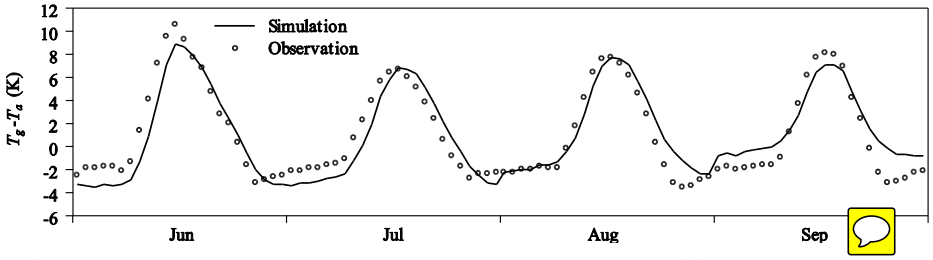

Figure 4 Comparison of the simulated and observed monthly mean diurnal variations in potential difference between surface temp erature (T_g) and air temperature (T_a).

difference between surface and air.

However, based on the above sensitivity analysis of the key parameters in the sensible heat flux calculation, the overestimation of the sensible heat flux and the underestimation of the latent heat flux in the A'rou meadow are much more likely to be caused by the latent heat flux calculation module rather than the sensible heat flux calculation module. This could be a result of the insufficiency of the evapotranspiration process simulation, which would lead to the underestimation of the latent heat flux.

2.2 Process analysis on latent heat flux underestimation

The estimation of latent heat flux is determined by the capability of soil evaporation and vegetation transpiration process modeling. The energy partition between the sensible and latent heat fluxes is unbiased in September, as seen from Figures 2(b) and 2(c). The bias occurs in June, July, and August. The monthly averaged LAI in A'rou meadow is the highest in July and August, all reaching 3.3, derived from MODIS LAI product. Because the simulation starts from June 11, the mean LAI in June used for modeling is 2.1, whereas the mean LAI in September is only 1.3, indicating a significant decrease from August to September. This information demonstrates that the vegetation grows best from June to August.

As the most significant difference between September and the other three months, i.e., June, July, and August, is the vegetation growth period, the negative bias in the latent heat flux estimation may be caused mainly by the insufficiency of the vegetation transpiration simulation. The transpiration simulation result is based on two aspects: the water content of the root layer soil and the intensity of physiological processes, including photosynthesis and respiration. Figure 5 shows that the root layer soil moisture is not underestimated. Instead, the decrease rate of simulations during dry periods is lower than that of observations. This indicates that the underestimation of the latent heat flux is not the result of the lack of soil water. One rational explanation is that the physiological process of vegetation has not been fully simulated and the transpiration is underestimated, which leads to the low decrease rate of the soil moisture.

The main parameter in vegetation physiological processes affecting transpiration is stomatal resistance (conductance), r_s (=1/g_s). Higher conductance yields higher canopy transpiration, as indicated by eq. (5a). In the first version of the SiB model, stomatal resistance is described by an empirical model without consideration of photosynthesis. However, the SiB2 model includes a photosynthesis-conductance model, which has a significant influence on vegetation photosynthesis and transpiration process modeling. The photosynthesis-conductance method calculates stomatal conductance g_s as a function of net assimilation rate A_n through eq. (5b). Net assimilation rate is calculated as the difference between the leaf assimilation rate and leaf respiration rate through eq. (5c). The leaf assimilation rate is the minimum of three limiting rates, shown in eq. (5d).

$$LE_{ct} = \left[\frac{e^*(T_c) - e_a}{1/g_c + 2r_b}\right]\frac{\rho c_p}{\gamma}(1 - W_c). \tag{5a}$$

$$g_s = m\frac{A_n}{c_s}h_s p + b. \tag{5b}$$

$$A_n = A - R_d. \tag{5c}$$

$$A \leqslant \mathrm{Min}(w_c, w_e, w_s). \tag{5d}$$

where $e^*(T_c)$ is the saturation vapor pressure at temperature T_a (Pa); e_a is the vapor pressure in canopy air space (Pa); g_c and g_s are the canopy stomatal conductance and leaf stomatal conductance, respectively (mol m^{-2} s^{-1}); γ is the psychrometric constant (Pa K^{-1}); W_c is the canopy wetness - snow cover fraction; m is the stomatal slope factor; c_s is the CO_2 partial pressure at leaf surface (Pa); h_s is the relative humidity at leaf surface; p is the atmospheric pressure (Pa); b is the minimal stomatal conductance (mol m^{-2} s^{-1}); A_n is the net assimilation rate (mol m^{-2} s^{-1}); A is the leaf photosynthetic rate (mol m^{-2} s^{-1}); R_d is the leaf respiration rate (mol m^{-2} s^{-1}); w_c is the Rubisco (leaf enzyme) limited rate of assimilation (mol m^{-2} s^{-1}); w_e is the light-limited rate of assimilation (mol m^{-2} s^{-1}); and w_s is the carbon compound export limitation or PEP-Carboxylase limitation on photosynthesis (mol m^{-2} s^{-1}).

Thus, the stomatal conductance is restricted by R_d and

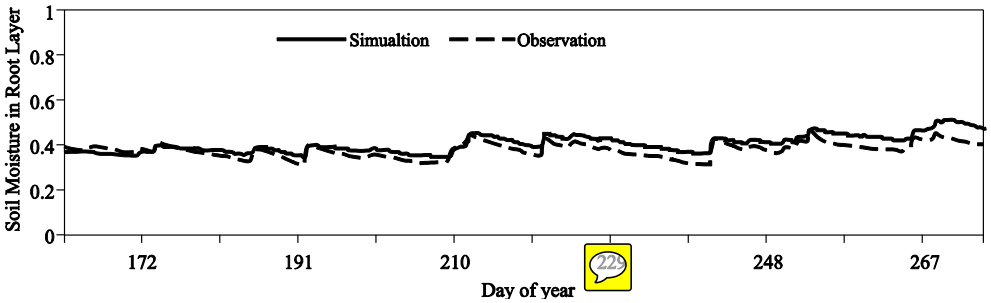

Figure 5 Comparison of the simulated and observed soil moisture (v/v) of the root layer (5–40 cm).

the three assimilation limitation components, w_c, w_e, and w_s. For type 6 vegetation, to which A'rou belongs, R_d, w_c, w_e, and w_s can be given as:

$$R_d = 0.025V_m, \tag{6a}$$

$$w_c = V_m, \tag{6b}$$

$$w_e = (\mathbf{F}_\pi \cdot \mathbf{n})\varepsilon_4(1-\omega_\pi), \tag{6c}$$

$$w_s = 2\times10^4 V_m c_i / p. \tag{6d}$$

where V_m is the maximum catalytic capacity of Rubisco (mol m^{-2} s^{-1}); $\mathbf{F}_\pi$ is the flux of Photosynthetically Active Radiation (PAR) incident on the leaf (W m^{-2}); $\mathbf{n}$ is the vector of leaf normal; ε_4 is the intrinsic quantum efficiency for CO_2 uptake (mol); ω_π is the leaf-scattering coefficient for PAR; c_i is the partial pressure of CO_2 in the leaf interior (Pa); p is the atmospheric pressure (Pa).

One main parameter related to the $\mathbf{F}_\pi \cdot \mathbf{n}$ is LAI, obtained from the MODIS product, which gives a reasonable value. V_m is a key parameter for the calculation of w_c and w_s. It is parameterized in the photosynthesis-conductance model as follow:

$$V_m = V_{\max} f_T(T_c) f_w(W_2), \tag{7}$$

where $V_{\max}$ is the maximum catalytic capacity of the leaf; $f_T(T_c)$ and $f_w(W_2)$ are two functions of canopy temperature and soil moisture, respectively.

As stated above, the soil moisture in the root layer has not been underestimated. Therefore, the problem may exist in $f_T(T_c)$, which is expressed as follows:

$$f_T(T_c) = 2Q_t / \{1+\exp[s_1(T_c - s_2)]\}, \text{ for } C_3V_m \tag{8a}$$

$$f_T(T_c) = 2Q_t / \{1+\exp[s_1(T_c - s_2)]\} \times\{1+\exp[s_3(s_4 - T_c)]\}, \text{ for } C_4V_m \tag{8b}$$

$$f_T(T_c) = 2Q_t / \{1+\exp[s_5(T_c - s_6)]\}, \text{ for } R_dV_m \tag{8c}$$

$$Q_t = (T_c - T_{opt})/10. \tag{8d}$$

where s_1 is the high temperature inhibition factor, photosynthesis (K^{-1}). s_2 is the half-inhibition high temperature (K). s_3 is the low temperature inhibition factor, photosynthesis (K^{-1}). s_4 is the half-inhibition low temperature (K). s_5 is the high temperature inhibition factor, respiration (K^{-1}). s_6 is the half-inhibition high temperature (K). T_{opt} is the optimum temperature for vegetation growth (K). There is no more detailed parameterization of T_{opt}. It is set to be 298 K (25°C).

In previous applications and evaluations, the rationality of the parameterization of $f_T(T_c)$ has not been fully considered. Under normal meteorological conditions, the optimum temperature for vegetation growth is relatively fixed and the inhibition parameters only vary with vegetation type. The SiB2 model classifies vegetation into nine types. Each type has a fixed set of temperature inhibition parameters. For instance, the A'rou meadow belongs to grass land type 6 (Sellers et al., 1996a), for which the half-inhibition high and low temperatures are set to be 313 and 288 K, respectively. This parameter setting, especially setting the optimum temperature for vegetation growth to 25°C for all vegetation types, might not be appropriate for extremely high-cold regions, such as A'rou. The air temperature from 11 to 18 June 2008, shown in Figure 6, indicates that most periods are under the default half-inhibition low temperature (288 K), below which vegetation should grow slowly. However, the MODIS-derived LAI data indicate that the vegetation grows well in June, July, and August. Therefore, the default setting of optimum and inhibition temperatures is not appropriate when the model is applied to extremely high-cold regions. Interestingly, Rosolem et al. (2010) also found that default inhibition parameters were not appropriate for simulations of tropical rainforest in an artificial ambient emulating characteristics of the Amazon in Biosphere 2.

As shown in eqs. (5a)–(5d), the insufficient simulation of vegetation physiological process leads to an underestimation of stomatal conductance, thereby leading to an underestimation of latent heat fluxes. The negative bias in latent heat fluxes will accordingly result in a positive bias in sensible heat fluxes by increasing the prognostic variable canopy temperature (T_c) through eqs. (1a) and (2a).

3 The modification of Vegetation Physiological Parameters and evaluation

Vegetation growth temperature range, denoted by optimum temperature and inhibition parameters, is related to the vegetation type and local climate (Lambers et al., 2008). For instance, the optimum temperature for *Notodanthonia penicillata* could be as high as 27.0°C, whereas that for *C. rigida* might be as low as 9.0°C. Growth temperature even varies within species, e.g., the maximum growth temperature of *Festuca novae-zelandiae* populations could be 18.0°C at low latitudes whereas this decreases to 12.0°C for populations at high latitudes (Scott, 1970).

To obtain accurate information on vegetation growth temperature for a certain region, some detailed information is required, such as species, structure of the local plant community, and growth temperature range of the species. However, obtaining such information is not practical owing to time and cost constraints. Most land surface models, including SiB2, classify vegetation cover into different types to simplify the parameterization schemes and make better use of the observed data, especially remote sensing data, for large-scale simulation and forecasting.

As discussed earlier, the default vegetation growth temperature range in the SiB2 model is not appropriate for simulating the climate features of extremely high-cold regions. Therefore, a relatively accurate and suitable scheme needs

to be formulated to obtain optimum and inhibition temperatures of vegetation growth in extremely high-cold region. Each of the various plant species around the world has their own growth temperature range. The local climate and environment select appropriate species to survive under unique circumstances, and plants growing under specific climate condition tend to adapt themselves to the local environment. There is abundant evidence indicating that plants adapt their photosynthetic process to local temperature through a process known as temperature acclimation (Badger et al., 1982; Berry and Bjorkman, 1980; Field et al., 1995; Seemann et al., 1984). The CASA (Carnegie-Ames-Stanford Approach) model (Field et al., 1995), for instance, calculates the optimum temperature by the mean temperature during the month of maximum NDVI. Cui (Cui, 2013) estimated the realistic optimum growth temperature in China and found that the lowest referenced optimum temperature, approximately 7°C, occurs in the Tibetan Plateau. In this study, we introduced a scheme that sets the average daytime temperature in the period with fast vegetation growth as the optimum growth temperature. The half-inhibition high and low temperatures are adjusted by the same temperature difference.

Recent studies on temperature reconstructions using tree-ring records show that the mean summer temperatures in the eastern Tibetan Plateau have been around 7 to 12°C for the past one thousand years (Fan et al., 2009; Li et al., 2012; Xu et al., 2011), indicating that summer temperature is consistently at least 13°C lower than 25°C for a long period. In this study, we calculate the average daytime temperature between June and July in 2007 and 2008, to be about 285 K, which is 13 K lower than the default value. The optimum and half-inhibition temperatures are then deducted 13 K from the default values as shown in Table 6. Figure 7 shows the simulated results with the adjusted temperature parameters. The biases in sensible heat flux and latent heat flux are clearly reduced. More specifically, simulated net radiation is generally consistent with the observations. The determination coefficient R^2 is 0.99 (RMSE=15.7 W m^{-2}), and the model slightly overestimates the net radiation, by ~1.4% according to the slope of the linear regression function. The sensible, latent, and soil heat fluxes are overestimated by 6.3%, 1.1%, and 4.4% respectively, which

Table 6 Adjusted temperature parameters

	T_{opt}	S_2	S_4	S_6
Temperatures (K)	285	300	275	315

is a considerable improvement over the previous simulations. The determination coefficient of sensible heat flux is only 0.52 (RMSE = 39.1 W m^{-2}). Nevertheless, there are several outliers, which increase the uncertainty. The simulated latent heat flux has a relatively high correlation with the observations. The determination coefficient is 0.86 (RMSE = 35.4 W m^{-2}). The uncertainty in soil heat flux simulations is relatively high, and the determination coefficient of the soil heat flux is only 0.40 (RMSE = 66.0 W m^{-2}). According to the scatter figure of the soil heat flux (Figure 7(d)), the dots located to the upper left of the 1 : 1 line are dominant, indicating that the positive soil heat flux (downward) is overestimated and some negative soil heat flux observations (upward) are shown to be positive in the simulations. However, the bias in the model simulations has been reduced significantly by correcting the optimum and inhibition temperature of vegetation growth. The sensible, latent, and soil heat fluxes seem to be overestimated, but here we have not accounted for the lack of energy balance closure (about 13%). Therefore, the errors in the simulated heat fluxes are within the range for uncertainties in the measured fluxes.

Figures 8((a)–(d)) shows the simulation results of each energy budget components at A'rou site from 19 to 23 June, 2008. The sensible heat flux is overestimated on 22 June, especially around noontime, viewed from Figure 8(b). But this situation does not appear in other days around 22 June. No significant bias exists in latent heat flux simulations, including 22 June (Figure 8(c)). However, there is a notable negative bias in soil heat flux on 22 June.

Figures 8((e)–(f)) depict the land surface radiative temperature, soil moisture in the root layer, and observed precipitation from 19 to 23 June. The surface temperature is underestimated to some extent, which should have caused a negative bias in both sensible heat flux and soil heat flux. However, the sensible heat flux is overestimated, and therefore, some energy that should be partitioned to soil heat flux has been assigned to sensible heat flux. This indicates that the energy transfer within the soil was not simulated well by the

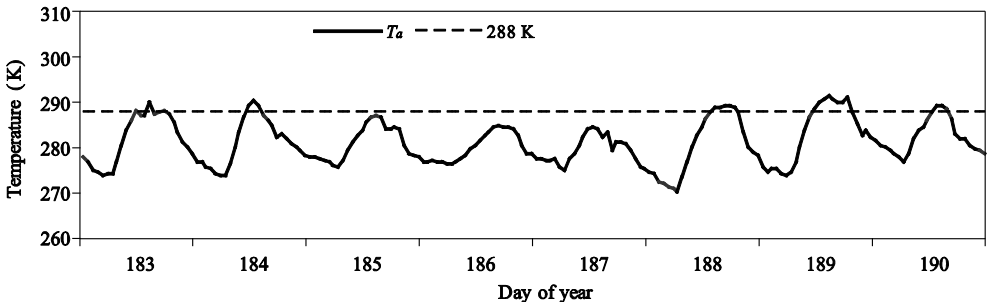

Figure 6 Observed air temperature at the A'rou site (at a 2-m height) from 11 to 18 June 2008

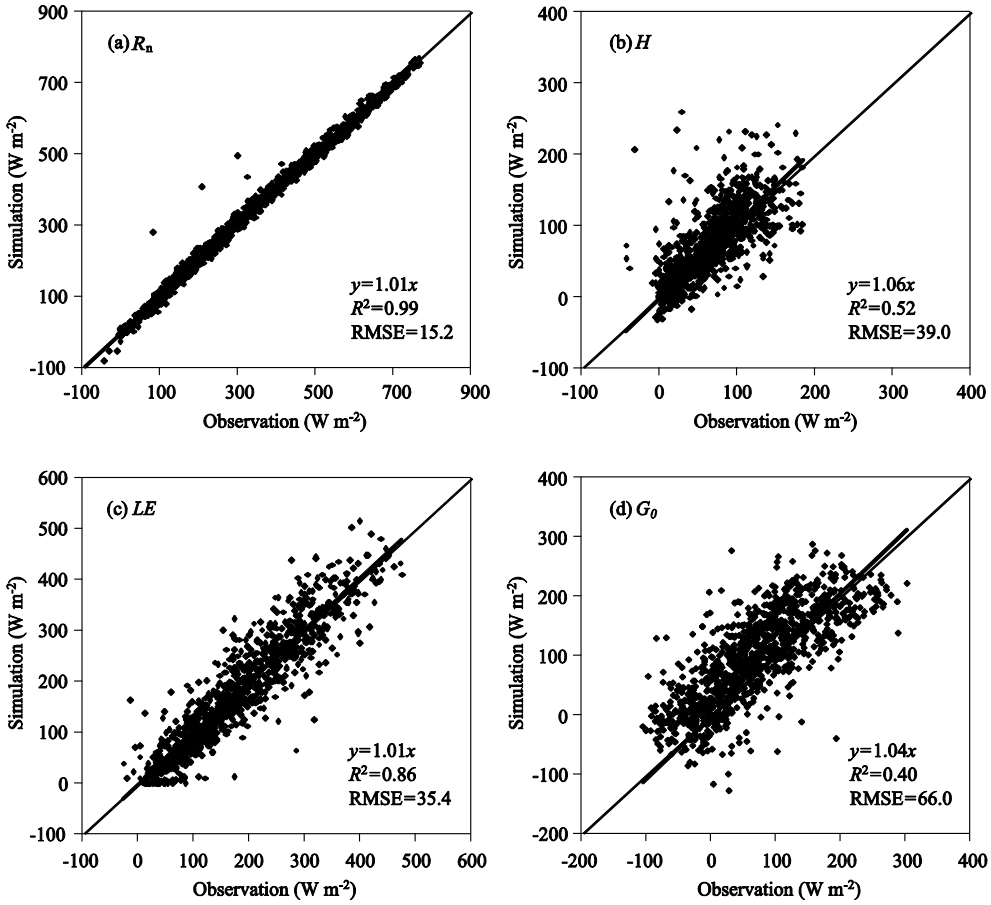

Figure 7 Scatter plots of the surface energy budget modeled with updated parameters against observations for an unstable stratification condition (daytime)

model.

Figure 8(f) shows that there were two rainfall events within these five days: one on the evening of 19 June and the other on the evening of 21 June, with the amounts of 8.8 mm and 13.5 mm, respectively. This led to an increase in the soil moisture and cloudlessness for a few days. The increase in the soil moisture is confirmed from the root layer soil moisture curve (Figure 8(f)). The high net radiation on 20 and 22 June indicates clear skies and high visibility after the rainfall events. The magnitudes of net radiation on 20 and 22 June were twice that of previous days, which should result in an increase in the sensible, latent, and soil heat fluxes. There is a clear increase in the observed values of the latent and soil heat fluxes, although the increase in the sensible heat flux is not significant. The trends shown from the observed data are reasonable. First, the increase in the soil moisture will cause an increase in evapotranspiration, which takes more energy away through latent hear flux. Second, it will cause an increase in the soil thermal conductivity, which in turn leads to an increase in the soil heat flux. The increases in the latent and soil heat fluxes will deplete most of the energy resulting from the increase in the net radiation, which in turn slows down the increase in the surface temperature. Moreover, the increase in the soil moisture will increase the soil thermal capacity, which further retards the soil temperature increase. Therefore, the observed data do not show a drastic increase in sensible heat flux.

This energy partition pattern shown in observed data has not been fully simulated by the model. From the simulation results, the soil heat flux did not show sufficient response to changes of the environment, and therefore, extra energy was partitioned to sensible heat flux. The insufficient simulation of the soil heat flux occurred because the impact on soil thermal conductivity is not sufficiently represented in the model. Another possible reason is that water was not retained long enough in the soil, which hindered the increase in the soil thermal conductivity. This may be related to the soil water and energy transfer processes, which are simulated with uniform values in all layers for stratified soil texture, porosity, and hydraulic conductivity (van der Velde et al., 2009; Yang et al., 2005). Although some studies have focused on this issue (Gao et al., 2007), improvements on parameterization of soil water and energy transfer process require more investigation.

Figure 9 provides another example of energy budget daily variation from 12 to 16, August 2008. The estimated energy budget components are in good agreement with the

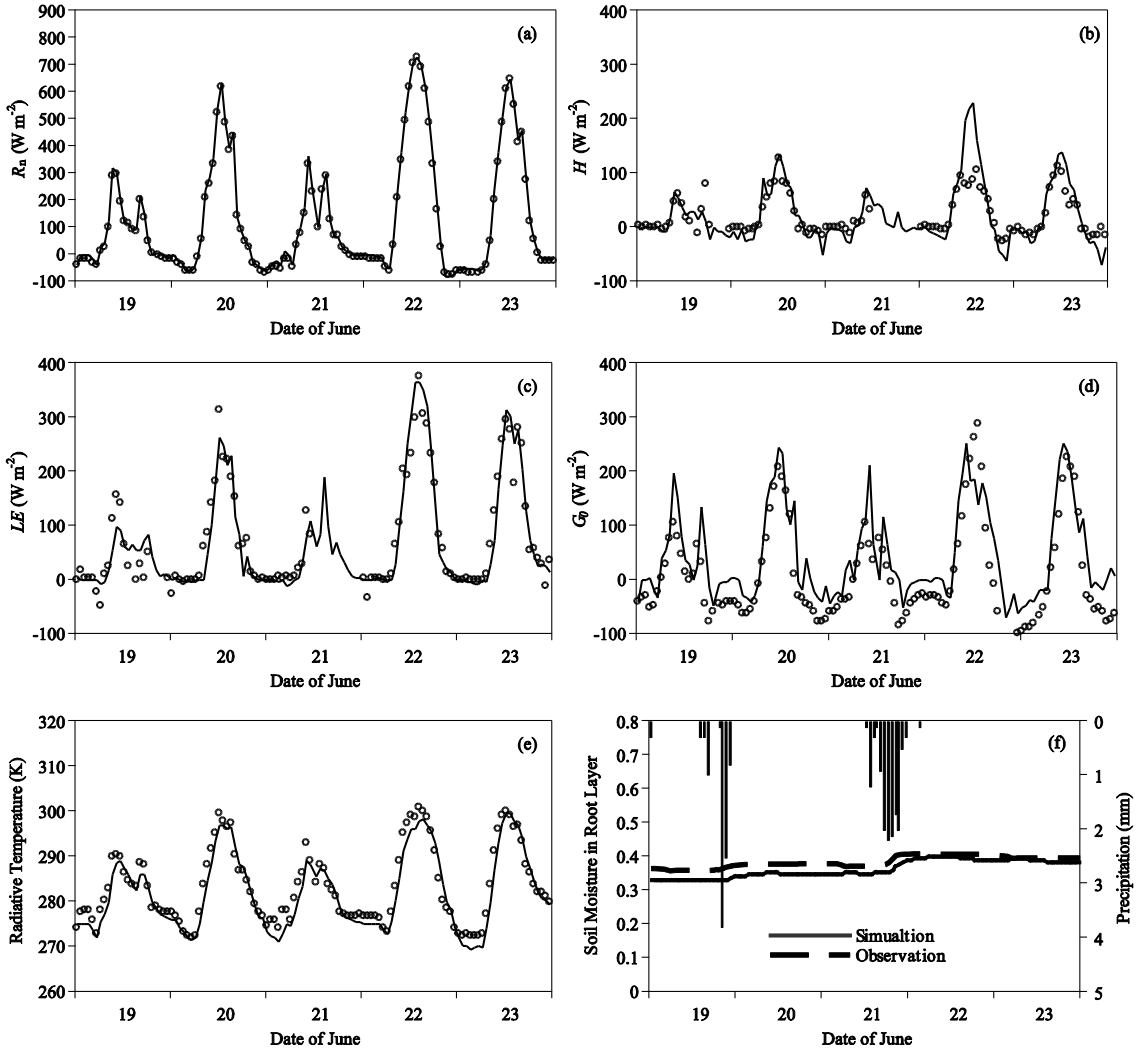

Figure 8 Simulation results from 19 to 23 June, 2008. Solid curves represent the simulation results. Circles (a–e) and the dashed curve (f) represent observed data. Bars in (f) represent the observed precipitation

observations, except for 15 August, as seen in Figures 9((b)–(f)). Both sensible and latent heat fluxes are overestimated in daytime, whereas the soil heat flux and land surface temperature are well estimated. Therefore, apart from the uncertainty of the model estimation, the energy closure problem of the flux observation is also a major source of the overall error. As shown in Figure 9(a), the net radiation was higher on 15 August than on 14 and 16 August. However, the observed sensible and soil heat fluxes are not higher and the observed latent heat flux is even lower on 15 August. Therefore, it can be inferred that there is a significant lack of energy balance closure in the observed data. Figure 9(f) shows the energy closure status of the observations in these five days. The difference between energy income and outcome (R_n–(H+LE+G_0)) is very large on 15 August. The daily energy balance ratio is only 59.78% on 15 August, whereas the ratios are above 75% on other days (Table 7). Thus, the difference between the observation and the simulation does not imply that the simulation is very biased.

Table 7 Energy balance closure of observations at A'rou site from 12 to 16 August, 2008

Date of August	12	13	14	15	16
Energy balance ratio (%)	80.9	82.3	93.9	59.8	75.1

4 Discussion and conclusion

We have simulated and evaluated the land surface energy budget at the A'rou meadow using AWS observations, EC observations, field surveys, and remote sensing data. The results obtained when using default vegetation physiological parameters show that the sensible, latent, and soil heat flux estimations have a 28% positive bias, a 13% negative bias, and a 7% positive bias, respectively. By analyzing the key parameters and states in the calculation of the sensible heat flux and latent heat flux, we identified that the bias was caused by selection of inappropriate optimum growth temperature and inhibition temperatures. In the SiB2 model,

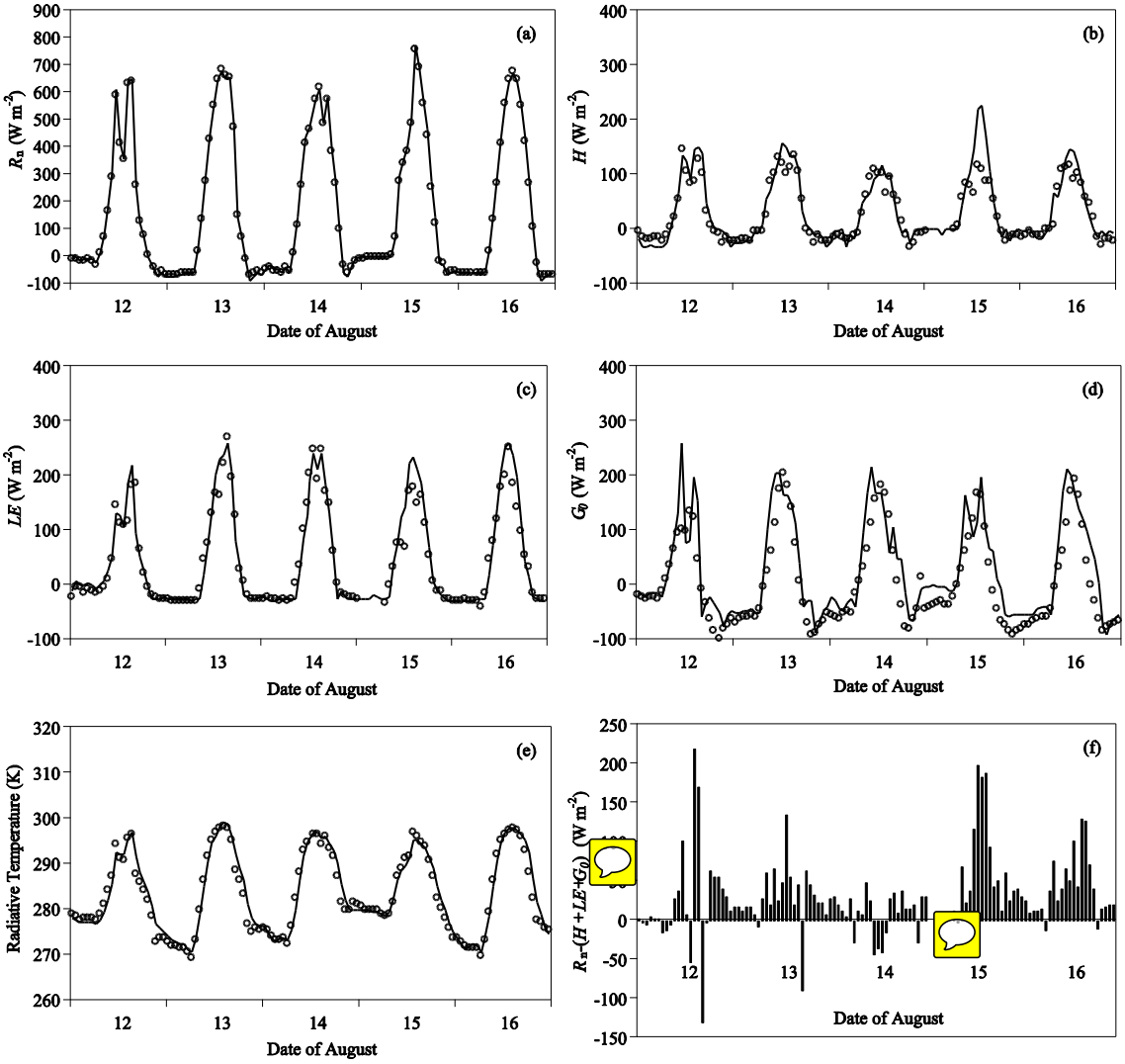

Figure 9 Simulation results from 12 to 16 August, 2008. Solid curves are simulations and circles are observations

the default optimum growth temperature is set as 298 K and inhibition temperatures are specified by the vegetation types. In general, these parameters do not change when the model is applied in different regions. However, this parameter setting is not appropriate for the eastern and central Tibetan Plateau. Although this region is at a high altitude and is extremely cold, there is a considerable precipitation during summer owing to the onset of the eastern Asian summer monsoon. Therefore, vegetation grows well during summer. Thus, an optimum growth temperature of 298 K is much higher than the actual maximum daily temperature in summer. In this study, the average daytime temperature during the period in which the vegetation growing fastest (June and July) was selected as the optimum growth temperature, and the inhibition temperatures were adjusted by the same level based on the optimum temperature. The biases in sensible, latent, and soil heat flux were reduced to a large extent (to less than 7% bias).

As previously stated, abundant evidence indicates that optimum/inhibition growth temperatures change with the environment temperature (Badger et al., 1982; Berry and Bjorkman, 1980; Cui, 2013; Field et al., 1995; Scott, 1970; Seemann et al., 1984). The physiological mechanism behind this is called temperature acclimation. This process is a constituent part of the ecological succession. Furthermore, there are other novel approaches to estimate optimum and inhibition temperatures for a large area, e.g., using remotely sensed vegetation information (Cui, 2013). Therefore, the best way for constructing vegetation growth temperature parameters in regional and global scale needs further assessments.

The process analysis is effective for identifying the parameter uncertainties and improving the land surface modeling. The advantages of this approach are that parameter adjustments are based on model responses to physical processes and that the model parameter set is reconstructed based on assumptions with physical implications. However, this procedure is conducted sequentially and sensitivity

analysis is essentially local analysis. Thus, one limitation of this scheme is that the interactions between parameters are not sufficiently considered, and this could have a significant impact on the overall uncertainty for complex models. One potential solution for addressing this issue is to estimate parameters using automatic global optimization approaches, e.g., the Genetic Algorithm (GA) (Wang, 1991), the Shuffled Complex Evolution (SCE) method (Duan et al., 1992), and Markov Chain Monte Carlo (MCMC) based methods (Kuczera et al., 2010; Vrugt et al., 2008). These methods are well known as model calibration tools. For instance, Zhu et al. (Zhu et al., 2013) also used A'rou data and modeled actual *ET* using a two-source model, but they resorted to an MCMC-based calibration approach to estimate parameters and found that the seasonal variation in canopy conductivity should be considered for extremely high-cold regions. However, calibration methods automatically search for parameter sets that fit observations, without due consideration of the physical implications of the parameters. Therefore, these methods are mostly implemented for conceptual models with fewer parameters and less strict physical implications (Gupta et al., 1998). Land surface models are mostly physically based and any changes in parameters should be assessed carefully with physical explanations, and this challenges the application of auto-calibration methods in land surface modeling. Few studies have shown that auto-calibration methods could improve the predictability of land surface models. These calibration works were carefully conducted for conceptualized parameters in models with strict constraints and multi-source observations (Crow et al., 2003; McCabe et al., 2005; Troy et al., 2008). Therefore, the next step is to investigate parameter auto-calibration approaches for improving the SiB2 simulation. One issue with this is that although the bias has been significantly reduced, the error has not been reduced considerably, as seen from R^2 and RMSE values. This is because adjusting parameters could correct the bias in flux estimation, but the overall uncertainty may come from multiple sources, e.g., initial state variables, forcing data, validating data, and model structure, in addition to parameters. The uncertainty could be further reduced by incorporating data assimilation scheme to correct error, before which our parameters setting scheme could be valuable to be implemented, as data assimilation methods should be based on the assumption of unbiased model and observation errors. Besides, further investigating water and energy transfer processes and improving the accuracy and precision of observations, especially eddy covariance data, are also important scientific tasks in future work.

This work was supported by the National Natural Science Foundation of China (Grant Nos. 91125002, 40971221) and FP7 CEOP-AEGI (Coordinated Asia European long-term observing system of the Qinhai Tibet Plateau hydro-meteorological processes and the Asian monsoon system with Ground satellite Image data and numerical simulation) project. We thank Dr. Tongren Xu and three anonymous reviewers for their thorough and constructive comments that significantly improved this paper.

Badger M R, Bjorkman O, Armond P A. 1982. An analysis of photosynthetic response and adaptation to temperature in higher plants: Temperature acclimation in the desert evergreen Nerium oleander L. Plant Cell Environ, 5: 85–99

Berry J, Bjorkman O. 1980. Photosynthetic response and adaptation to temperature in higher plants. Annu Rev Plant Physiol, 31: 491–543

Chen Y Y, Yang K, He J, et al. 2011. Improving land surface temperature modeling for dry land of China. J Geophys Res, 116: D20104, doi: 10.1029/2011jd015921

Chen Y Y, Yang K, Tang W J, et al. 2012. Parameterizing soil organic carbon's impacts on soil porosity and thermal parameters for Eastern Tibet grasslands. Sci China-Earth Sci, 55: 1001–1011

Chen Y Y, Yang K, Zhou D, et al. 2010. Improving the Noah land surface model in arid regions with an appropriate parameterization of the thermal roughness length. J Hydrometeorol, 11: 995–1006

Crow W T, Wood E F, Pan M. 2003. Multiobjective calibration of land surface model evapotranspiration predictions using streamflow observations and spaceborne surface radiometric temperature retrievals. J Geophys Res, 108: D234725, doi: 10.1029/2002jd003292

Cui Y P. 2013. Preliminary estimation of the realistic optimum temperature for vegetation growth in China. Environ Manage, 52: 151–162

Duan Q, Sorooshian S, Gupta H V. 1992. Effective and efficient global optimization for conceptual rainfall-runoff models. Water Resour Res, 28: 1015–1031

Fan Z X, Bräuning A, Yang B, et al. 2009. Tree ring density-based summer temperature reconstruction for the central Hengduan Mountains in southern China. Glob Planet Change, 65: 1–11

Field C B, Randerson J T, Malmström C M. 1995. Global net primary production: Combining ecology and remote sensing. Remote Sens Environ, 51: 74–88

Gao Z Q, Bian L G, Cheng Y J, et al. 2002. Modeling of energy budget using Simple Biosphere Model version2(SiB2) over Tibetan Naqu Prairie. J Appli Meterol Sci, 13: 129–141

Gao Z Q, Chae N, Kim J, et al. 2004. Modeling of surface energy partitioning, surface temperature, and soil wetness in the Tibetan prairie using the Simple Biosphere Model 2 (SiB2). J Geophys Res, 109: D06102, doi: 10.1029/2003JD004089

Gao Z Q, Chen G T J, Hu Y B. 2007. Impact of soil vertical water movement on the energy balance of different land surfaces. Int J Biometeorol, 51: 565–573

Gupta H V, Sorooshian S, Yapo P O. 1998. Toward improved calibration of hydrologic models: Multiple and noncommensurable measures of information. Water Resour Res, 34: 751–763

Hanan N P, Berry J A, Verma S B, et al. 2005. Testing a model of CO_2, water and energy exchange in Great Plains tallgrass prairie and wheat ecosystems. Agric For Meteorol, 131: 162–179

Hong J, Kim J. 2010. Numerical study of surface energy partitioning on the Tibetan plateau: Comparative analysis of two biosphere models. Biogeosciences, 7: 557–568

Hu H P, Ye B S, Zhou Y H, et al. 2006. A land surface model incorporated with soil freeze/thaw and its application in GAME/Tibet. Sci China Ser D-Earth Sci, 49: 1311–1322

Koike T. 2004. The coordinated enhanced observing period-An initial step for integrated global water cycle observations. WMO Bull, 53: 115–121

Koike T, Yasunari T, Wang J, et al. 1999. GAME-Tibet IOP summary report. In: Proceedings of the First International Workshop on GAME-Tibet, Xi'an, China, 1–2

Kuczera G, Kavetski D, Renard B, et al. 2010. A limited-memory acceleration strategy for MCMC sampling in hierarchical Bayesian calibration of hydrological models. Water Resour Res, 46: W07602, doi: 10.1029/2009wr008985

Lambers H, Chapin III F S, Pons T L. 2008. Plant Physiological Ecology. New York: Springer

Li Q, Sun S F. 2008. Development of the universal and simplified soil model coupling heat and water transport. Sci China Ser D-Earth Sci, 51:

88–102
Li Q, Sun S F, Xue Y K. 2010. Analyses and development of a hierarchy of frozen soil models for cold region study. J Geophys Res, 115: D03107, doi: 10.1029/2009jd012530
Li X, Cheng G D, Liu S M, et al. 2013. Heihe Watershed Allied Telemetry Experimental Research (HiWATER): Scientific objectives and experimental design. Bull Amer Meteorol Soc, 94: 1145–1160
Li X, Koike T. 2003. Frozen soil parameterization in SiB2 and its validation with GAME-Tibet observations. Cold Reg Sci Tech, 36: 165–182
Li X, Li X W, Li Z Y, et al. 2009. Watershed allied telemetry experimental research. J Geophys Res, 114: D22103, doi: 10.1029/2008jd011590
Li Z S, Zhang Q B, Ma K P. 2012. Tree-ring reconstruction of summer temperature for A.D. 1475–2003 in the central Hengduan Mountains, Northwestern Yunnan, China. Clim Change, 110: 455–467
Liu S M, Xu Z W, Wang W Z, et al. 2011. A comparison of eddy-covariance and large aperture scintillometer measurements with respect to the energy balance closure problem. Hydrol Earth Syst Sci, 15: 1291–1306
Ma Y M, Kang S C, Zhu L P, et al. 2008. ROOF OF THE WORLD: Tibetan observation and research platform Atmosphere–Land interaction over a heterogeneous landscape. Bull Amer Meteorol Soc, 89: 1487–1492
McCabe M F, Franks S W, Kalma J D. 2005. Calibration of a land surface model using multiple data sets. J Hydrol, 302: 209–222
Prihodko L, Denning A S, Hanan N P, et al. 2008. Sensitivity, uncertainty and time dependence of parameters in a complex land surface model. Agr Forest Meteorol, 148: 268–287
Qiu J. 2008. China: The third pole. Nature, 454: 393–396
Rosolem R, Shuttleworth W J, Zeng X, et al. 2010. Land surface modeling inside the Biosphere 2 tropical rain forest biome. J Geophys Res, 115: G04035, doi: 10.1029/2010jg001443
Scott D. 1970. Relative growth rates under controlled temperatures of some New Zealand indigenous and introduced grasses. N Z J Bot, 8: 76–81
Seemann J R, Berry J A, Downton W J S. 1984. Photosynthetic response and adaptation to high temperature in desert plants. Plant Physiol, 75: 364–368
Sellers P J, Los S O, Tucker C J, et al. 1996a. A revised land surface parameterization (SiB2) for atmospheric GCMs. PartII: The generation of global field of terrestrial biophysical parameters from satellite data. J Clim, 9: 706–737
Sellers P J, Randall D A, Collatz G J, et al. 1996b. A revised land surface parameterization (SiB2) for atmospheric GCMs. PartI: Model formulation. J Clim, 9: 676–705
Sen O L, Shuttleworth W J, Yang Z L. 2000. Comparative evaluation of BATS2, BATS, and SiB2 with Amazon data. J Hydrometeorol, 1: 135–153
Song J H, Kang H S, Byun Y H, et al. 2010. Effects of the Tibetan Plateau on the Asian summer monsoon: A numerical case study using a regional climate model. Int J Climatol, 30: 743–759
Takayabu I, Takata K, Yamazaki T, et al. 2001. Comparison of the four land surface models driven by a common forcing data prepared from GAME/Tibet POP'97 products-snow accumulation and soil freezing processes. J Meteorol Soc Jpn, 79: 535–554
Troy T J, Wood E F, Sheffield J. 2008. An efficient calibration method for continental-scale land surface modeling. Water Resour Res, 44: W09411, doi: 10.1029/2007wr006513
van der Velde R, Su Z, Ek M, et al. 2009. Influence of thermodynamic soil and vegetation parameterizations on the simulation of soil temperature states and surface fluxes by the Noah LSM over a Tibetan plateau site. Hydrol Earth Syst Sci, 13: 759–777
Vrugt J A, ter Braak C J F, Clark M P, et al. 2008. Treatment of input uncertainty in hydrologic modeling: Doing hydrology backward with Markov chain Monte Carlo simulation. Water Resour Res, 44: W00B09, doi: 10.1029/2009wr008985
Wang Q J. 1991. The genetic algorithm and its application to calibrating conceptual Rainfall-Runoff Models. Water Resour Res, 27: 2467–2471
Watanabe T, Kondo J. 1990. The influence of canopy structure and density upon the mixing length within and above vegetation. J Meteorol Soc Jpn, 68: 227–235
Wilson K, Goldstein A, Falge E, et al. 2002. Energy balance closure at FLUXNET sites. Agr Forest Meteorol, 113: 223–243
Xu G B, Chen T, Liu X H, et al. 2011. Summer temperature variations recorded in tree-ring δ^{13}C values on the northeastern Tibetan Plateau. Theor Appl Climatol, 105: 51–63
Xu X D, Zhang R H, Shi X H, et al. 2008. A new integrated observational system over the Tibetan Plateau. Bull Amer Meteorol Soc, 89: 1492–1496
Yanai M, Li C F, Song Z S. 1992. Seasonal heating of the Tibetan Plateau and its effects on the evolution of the Asian summer monsoon. J Meteorol Soc Jpn, 70: 319–351
Yang K, Chen Y Y, Qin J. 2009. Some practical notes on the land surface modeling in the Tibetan Plateau. Hydrol Earth Syst Sci, 13: 687–701
Yang K, Koike T, Fujii H, et al. 2002. Improvement of surface flux parametrizations with a turbulence-related length. Q J R Meteorol Soc, 128: 2073–2087
Yang K, Koike T, Ishikawa H, et al. 2004. Analysis of the surface energy budget at a site of GAME/Tibet using a single-source model. J Meteorol Soc Jpn, 82: 131–153
Yang K, Koike T, Ye B S, et al. 2005. Inverse analysis of the role of soil vertical heterogeneity in controlling surface soil state and energy partition. J Geophys Res, 110: D08101, doi: 10.1029/2004jd005500
Yang K, Wang J M. 2008. A temperature prediction-correction method for estimating surface soil heat flux from soil temperature and moisture data. Sci China Ser D-Earth Sci, 38: 243–250
Yasunari T J, Koster R D, Lau K M, et al. 2011. Influence of dust and black carbon on the snow albedo in the NASA Goddard Earth Observing System version 5 land surface model. J Geophys Res, 116: D02210, doi: 10.1029/2010jd014861
Zhang G Z, Xu X D, Wang J Z. 2000. A dynamic study on PBL characteristics by '98 SCSMEX and TIPEX data. The Second Session of International Workshop on TIPEX-GAME/Tibet, Kunming, China. 58–60
Zhou D G, Huang R H. 2012. Response of water budget to recent climatic changes in the source region of the Yellow River. Chin Sci Bull, 57: 2155–2162
Zhu G F, Su Y H, Li X, et al. 2013. Estimating actual evapotranspiration from an alpine grassland on Qinghai-Tibetan plateau using a two-source model and parameter uncertainty analysis by Bayesian approach. J Hydrol, 76: 42–51